Numerical optimization of AdBlue®-injection into the mixing section of SCR-systems

Lukas Möltner,
Verena Schallhart
Department of Technologies and Life Sciences
Management Center Innsbruck
Maximilianstrassse 2, A-6020 Innsbruck
AUSTRIA
lukas.moeltner@mci.edu https://www.mci.edu

Abstract: The selective catalytic reduction (SCR) of nitrogenous oxides is the most promising technique to meet prospective emission regulations of cars. Due to its toxic potential the reducing agent ammonia cannot be stored in a car, but it can be carried in the form of an urea-water-solution (UWS) which is injected into the hot exhaust gas and reacts in different sub-steps to ammonia. This formation of ammonia upstream the catalytic converter is a key factor for the efficiency of the entire SCR-process-chain.

This study deals with the numerical optimization of the position and direction of the UWS-injection into the hot exhaust gas. For this purpose a numerical model was developed, which considers in contrast to previous surveys the loss of droplets` weight caused by evaporation and thermal decomposition. The model is able to determine the exact position of flying droplets, the droplets' velocity, the composition and its current temperature in a gas flow. Comparative investigations of coflow- and counter flow-injection, of centered or off-centered injection position of the UWS-injection system to avoid droplet/wall-contact are focused in this survey.

Key-Words: Exhaust gas after-treatment, internal combustion engines, NO_x, SCR, AdBlue®

1 Introduction

Diesel engines in combination with modern charging and diesel injection systems present constant high torque over a wide speed range and therefore excellent driving performance. These characteristics increased their popularity compared to gasoline engines. At present, almost 50% of all passenger cars in Europe are diesel-driven [1]. However, a major challenge in the future is to satisfy increasingly stringent emission regulations without dramatically rising costs of diesel engines [2]. Particularly the strictly limited nitrogen oxide (NO_x) emissions require great efforts.

Currently, the most effective technology to reduce NO_x emissions is the selective catalytic reduction (SCR) with ammonia. Due to the fact that a separate reducing agent tank is required to use SCR technology in cars and possible leaks in the tank and piping system can be classified as very harmful because of the toxicity of ammonia, only SCR-systems with NH_3-releasing substances are available or developed. These substances, e.g. urea, feature a clearly smaller toxicity and can be stored and dosed as an aqueous solution accordingly. At present, a distribution network, for the standardized urea-water-solution (UWS) according to DIN 70700, is established. UWS contains 32,5 wt.-% urea and is sold under the brand name AdBlue®.

The determining factor for the efficiency of SCR-systems, for a moderate reducing agent consumption and for meeting space requirements, is the sufficient ammonia generation and homogenization upstream the catalytic converter.

Subsequently to the evaporation of water out of the UWS droplets and the melting of urea, the formation of ammonia occurs, which is described in two single reactions. In the first reaction Eq. (1), a thermolytic decomposition of urea to ammonia and isocyanic acid takes place. Another mole of ammonia and CO_2 are produced from the isocyanic acid by hydrolysis, Eq. (2).

$$(NH_2)_2CO \leftrightarrow NH_3 + HNCO \quad (1)$$

$$HNCO + H_2O \leftrightarrow NH_3 + CO_2 \quad (2)$$

The single steps which occur between the UWS-injection and the entrance in the catalytic converter are shown in the process chain below, figure 1.

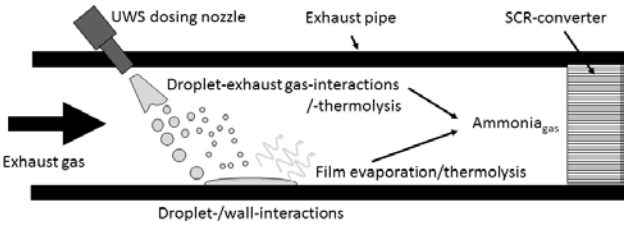

Fig. 1: Process chain of a SCR-system

The objective of this study is to optimize the UWS-injection into a simplified mixing section to achieve direct evaporation and thermolysis of a free moving droplet without any wall contact.

In detail, the angle of the injection nozzle and the direction of injection will be observed by numerical simulation under accurate consideration of occurring droplet/gas-interactions. Especially the influence of a counter flow injection to the droplet evaporation should be investigated.

The distinction from previous studies is the basic consideration of all relevant individual processes during ammonia formation and homogenization. The results of these investigations shall provide a basis for the development of highly effective mixing sections for SCR-systems.

2 Fundamentals

The droplet-motion-model is based on the balance of forces acting on a droplet in a gas flow, figure 2. This balance provides the basis for the equation of motion and further for the multi-dimensional motion model, which considers each spatial-axis and thus determines the droplet velocity and the droplet position. The starting point is the droplet movement with an initial velocity and directed motion.

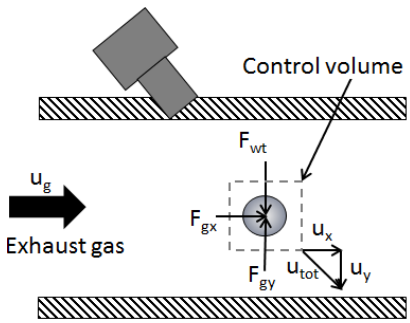

Fig. 2: Balance of forces at a moving droplet

In total, the sum of the single gas forces F_g and the weight F_{wt} are acting on a moving droplet and cause a change in its velocity $d\vec{u}_{dr}/dt$, Eq. (3), according to Newton's principle of action.

$$m_{dr}\frac{d\vec{u}_{dr}}{dt} = \vec{F}_g + \vec{F}_{wt} \quad (3)$$

The gas force F_g is the product of the projected area A_{pr}, the drag coefficient for drops c_{dr} and the dynamic pressure. The calculation of the drag coefficient requires the calculation of the Reynolds number, which is determined by the droplet diameter D_{dr}, the exhaust gas density ρ_g and the dynamic viscosity u_g. For droplets with a Reynolds number $Re_{dr} < 800$ Eq. (4) is applicable.

$$c_{dr} = \frac{24}{Re_{dr}}\left(1+0{,}15*Re_{dr}^{\,0{,}687}\right) \quad (4)$$

For Reynolds numbers $Re_{dr} > 800$ Eq. (5) comes into effect [3].

$$c_{dr} = 0{,}44 \quad (5)$$

The acting force of gravity and lift force F_{wt} is calculated by the drop volume V_{dr}, the droplet density ρ_{dr} and the gas density ρ_g. Insertions and transformations lead to Eq. (6), which describes after integration the drop velocity.

$$\frac{d\vec{u}_{dr}}{dt} = \frac{3}{4}*\frac{\mu_g * c_{dr} * Re_{dr}}{\rho_{dr} * D_{dr}^{\,2}}*\left(\vec{u}_g - \vec{u}_{dr}\right)+\left(1-\frac{\rho_g}{\rho_{dr}}\right)*\vec{g} \quad (6)$$

The motion vector is the result of re-integration, Eq. (7):

$$\frac{d\vec{x}_{dr}}{dt} = \vec{u}_{dr} \quad (7)$$

This equation is the basis for the presented simulation model and is state of the art for describing droplets' motion, e.g. [4]. However, this model only considers droplets with constant mass as well as constant material characteristics and temperature without observing changes caused by evaporation or chemical reactions. The next chapter presents the implementation of an evaporation model and a kinetic approach to extend the capabilities of the model.

3 Methodology

3.1 Experimental setup

In the course of the investigations a reference-geometry of the injection nozzle and the mixing section was defined. The mixing section, which is shown in figure 3, represents a simplified mixing section to understand the basic processes and to avoid unexpected interactions which may occur at more complex geometries.

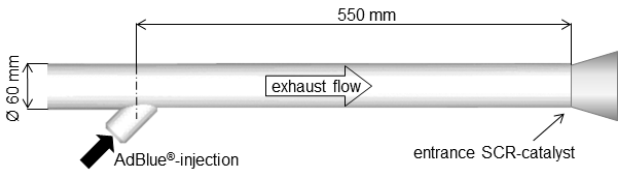

Fig. 3: Geometry of the simplified mixing section with an injection angle of 45° and an off-centered injection

The temperature of the exhaust gas and its flow velocity seriously influences the trajectories of the droplets and depends on the current operation point (OP) of the diesel engine. To cover a broad range of operating conditions following operation points were chosen, table 1:

Table 1: Exhaust gas mass flow and gas temperature of the investigated operation points

	mass flow [kg/h]	temperature [K]
OP 1	100	523
OP 2	350	723
OP 3	900	773

Initial spray parameters of the injection nozzle like the exit velocity or cone angle size distribution were determined empirically by high speed recordings and laser diffraction.

3.2 Modeling the droplet motion

The motion of droplets or spherical particles can fundamentally be described by Eq. (7). As mentioned above, this equation is only suitable when describing droplets with constant mass. In case of a change in mass and size due to evaporation and/or thermal decomposition the capabilities of the model have to be extended by these two sub-processes.

3.2.1 Droplet evaporation

A Lagrangian approach was chosen for the simulation of sprays. In this approach the calculation of droplets' trajectories, heat and mass transfer is only considered for a statistically representative number of drops inside a magnitude instead of the whole droplet collective.

Nusselt describes the evaporation as a diffusion phenomenon in a thin interphase between the droplet and the surrounding gas, subjected to the condition that the relative humidity of the surrounding gas is <1. Furthermore, the evaporation occurs faster if the droplet is continuously circulated by gas compared to a statically gaseous atmosphere.

Eq. (8) describes the mass transfer coefficient k_M, which is determined by the dimension-less Sherwood number Sh, the diffusion coefficient D, the Reynolds number Re_{dr} for droplets and the Schmidt number Sc. This equation was defined by experiments with drops of different liquids and diameter classes by Ranz and Marshall [5].

$$Sh_{(t)} \equiv \frac{k_M * D_{dr(t)}}{D} = 2 + 0,6 * Re_{(t)}^{\frac{1}{2}} * Sc^{\frac{1}{3}} \qquad (8)$$

Subsequently the mass loss rate of droplets due to evaporation can be calculated by Eq. (9). The diffusion of vapor in the exhaust gas occurs on the droplets' surface A_{sf}. This is quantitatively influenced by the mass transfer coefficient k_M and the driving force for diffusion phenomena is the vapour pressure $p_{v(Tg)}$.

$$\frac{dm_{(t)}}{dt} = -\frac{k_M}{R}\left[\frac{p_{v(T_{dr},t)}}{T_{dr(t)}} - \frac{X_g * p_{v(T_g)}}{T_g}\right] * A_{sf(t)} * M_{H2O} \qquad (9)$$

3.2.2 Non-isothermal decomposition of urea

Once the droplets are injected into the exhaust gas stream, convective heat transfer from the surrounding gas to the droplets occurs and thus evaporation starts. A direct decomposition of urea from the aqueous urea solution only takes place in a very limited extent. More likely there is a separation of urea and water prior to the formation of ammonia which takes place in two reaction steps according to Eq. (1) and (2). The quantitative description of the thermolytic decomposition according to Eq. (1) takes place by the application of a mathematic power law, Eq. (10). This power law describes the connection between the reaction rate r, the reaction rate constant $k_{therm(T)}$ and the reacting agent concentration c_{urea}.

$$r_{(k,c_{Urea})} = k_{therm(T)} * c_{urea}^{\ n} \qquad (10)$$

The temperature dependency of the reaction rate constant for thermolysis is calculated according to Arrhenius, Eq. (11) [6].

$$k_{therm} = 4,9 * 10^3 * \exp\left(-\frac{23066}{R * T}\right) \qquad (11)$$

The adjusting temperature within the droplet is calculated by the balance of heat, which depends on the exhaust gas temperature and the heat consumption due to the endothermic reaction, Eq. (12).

$$\frac{dT}{dt} = \frac{k_w * A_{sf} * \left(T_g - T\right) + \left(m_{dr\,0} - m_{dr(t)}\right) * \left(-H_{therm}\right)}{m_{dr(t)} * c_{p\,dr(t)}} \qquad (12)$$

As a result, the simulation model is finally able to take mass losses due to evaporation and/or chemical reaction into consideration. Therefore, a more precise calculation of the droplets' motion can be performed. The final computation was carried out by a conventional numerical solver based on Euler.

4 Discussion of results

4.1 Theoretical consideration of evaporation and decomposition of a stationary droplet

To enhance the knowledge of the chronological sequence of ammonia generation in SCR-systems the first simulations were performed for non-moving, static droplets. To illustrate the difference in the behavior of UWS and water the calculations were done for a pure water droplet too.

The result of the simulations, depicted in figure 4, show a sharp temporal delimitation of the sub-steps during ammonia formation. The graphs show the calculated profile of the droplets mass for a droplet of pure water, an UWS-droplet and the time-dependent mass fraction of pure urea in the UWS-droplet.

The reason for the faster weight loss of the water droplet can be found in the missing lowering of vapor pressure by the dissolved urea.

Additionally the progress of the droplet temperature is shown for the urea-water mixture. The evaporation of water out of a UWS droplet is described to be isothermal by Wozniak in [7]. The total amount of heat, which is transferred from the exhaust gas to the droplet, is used for evaporation and the temperature in the droplet remains at a steady state level. After the demixing-phase of water and urea in the droplet, recognizable by the mass fraction of urea achieving 1, the droplet's temperature increases. With increasing temperature of the droplet the reaction rate constant of the thermolysis increases too and accelerates the reaction. A second steady state level is reached as soon as a thermal equilibrium in the droplet between heat input by the exhaust gas and the applied heat of reaction is adjusted. This steady state temperature is very close to the ambient gas temperature. The reason for this is due to the high heat transfer between exhaust gas and droplet and the moderate required heat for the reaction [8].

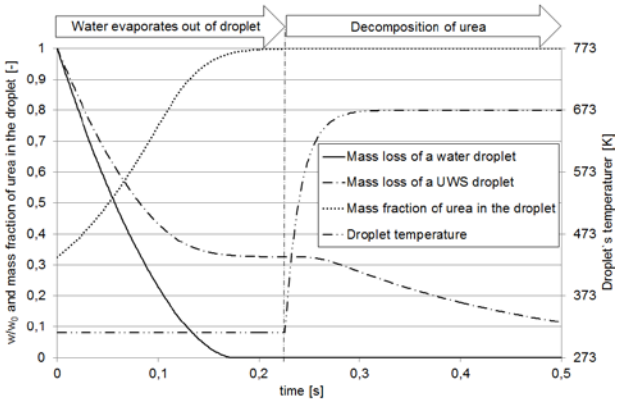

Fig. 4: Graphs of the droplet`s mass of pure water and UWS and the droplet temperature of UWS calculated at $T_g = 600$ K, initial droplet temperature $T_{dr} = 303$ K, $u_{rel} = 0$ m/s, $D_{dr0} = 70$ µm, $k_0 = 4{,}9 * 10^3$ 1/s and $E_{A\ Therm} = 23.066$ J/mol [8]

4.2 Trajectories of a free-moving droplet

The results of the preliminary study with a stationary droplet in figure 4 show that, depending on the initial droplet size the droplet evaporation as well as the thermal decomposition of urea result in significant weight losses.

This theoretical analysis explains the effect of the decreasing droplet mass to the droplets` trajectory of a free-moving droplet in a gas flow.

Figure 5 shows comparatively the results of four different approaches for the motion of a single droplet. It gets injected into a hot gas flow with an angle of 45° and an initial velocity of 25 m/s. It shows the distance, which the single droplet travelled in the axial as well as radial direction for:

- a droplet with constant mass,
- a pure water droplet,
- an UWS-droplet including evaporation of water,
- an UWS-droplet including mass losses caused by evaporation and thermolytic decomposition.

It depicts that the trajectories differ clearly for the droplet with constant mass, a pure water droplet from the flight paths of a droplet with evaporation and thermolysis. In particular, the trajectory of the droplet with constant mass reaches a substantially larger depth of penetration into the exhaust gas flow as all other models. In contrast, the pure water droplet achieves due to the large weight loss a much lower penetration depth. The precise calculation of this penetration depth is the key to design mixing sections with or without significantly reduced wall contact of droplets.

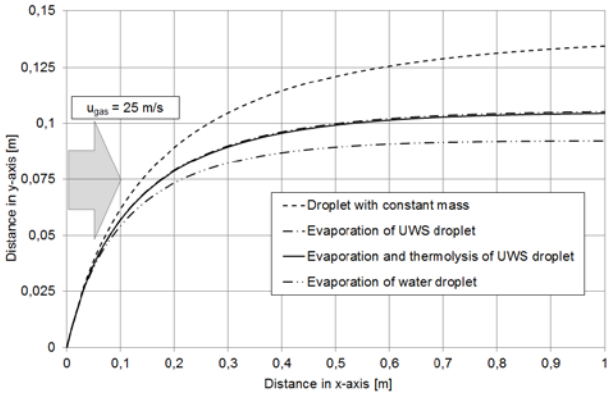

Fig. 5: Trajectories of different droplets each with an initial diameter D_{dr0} = 70 µm at T_g = 600 K, initial droplet temperature T_{dr} = 303 K, u_g = 25 m/s, injection angle 45°, initial droplet velocity of 25 m/s, k_{0Therm} = 4,9 * 10^3 1/s and $E_{A\ Therm}$ = 23.066 J / mol [9]

The comparison demonstrates that calculations which are based on droplets with constant mass result in noticeable deviations of the trajectories of UWS-droplets. Simplified simulations, working with the properties of pure water, are also subject to inaccuracies. The reason for these inaccuracies is the already mentioned lack of lowering vapor pressure by dissolved urea, which leads to a too rapid weight loss and a disproportionately strong deflection by the gas flow. The two models which are working with the properties of UWS and including evaporation and/or evaporation and thermolysis show only marginal differences in the trajectories. The reason for this is the chosen initial droplet diameter for this comparison. This is caused by the fact that the thermal decomposition of urea plays only a minor role to the weight loss, whereas the droplet evaporation dominates.

4.3 Model validation and plausibility check

To prove the validity of the simulation model, an empiric experiment using laser diffraction was carried out. For this purpose the droplet size distribution in the mixing zone was determined 15 cm downstream of the UWS-injection position.
According to the model-based calculations a small part of the droplet spectrum must follow directly the exhaust gas flow and can be detected by laser diffraction. Droplets of larger diameter classes are undetectable because of its inertia they interpenetrate the exhaust flow, hit the opposite wall and deposit there, figure 6.

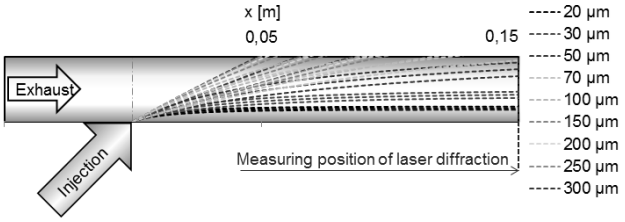

Fig. 6: Simulated droplet´s trajectories till the measuring position of laser diffraction

Figure 7 shows the comparison of the results of the simulation model and the experimental output. The experiment and the simulation results show that the droplets` size distribution decreases significantly 15 cm downstream the UWS-injection, which is explainable with the wall contact and deposition of bigger size classes of the initial droplet spectrum.

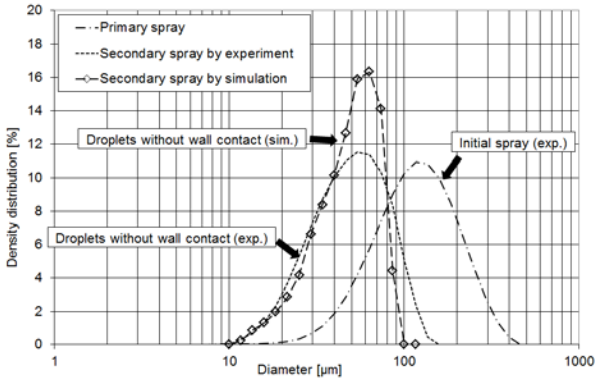

Fig. 7: Size distributions of the primary spray compared with the measured and calculated secondary spray after wall contact [9]

The comparison shows generally a good conformity of the diameter classes which are able to follow the exhaust gas flow between the model-based calculations and the experiment. Only the relative frequency around the relative maximum shows inaccuracies. The reason for this might be the method of analysis with discrete diameter classes and on the other hand deviations caused by the resolution of the laser diffraction measurement.

4.4 Model-based variation of injection position and direction

The reference scenario for the following optimization is represented by figure 8. The injection takes place with an angle of 45° (coflow) and is injected at the pipe wall (off-centered). The geometry of the injection nozzle could be determined as a three-jet-nozzle with a cone angle of 16° and a symmetrical jet-offset of 120°.

4.4.1 Coflow-injection off-centered (baseline)

Figure 8 shows the trajectories of different initial droplet sizes for the three observed operation points. Due to higher gas velocities the deflection of droplets increases with higher exhaust gas flow rates.

The figure shows furthermore that only droplets with small diameters can follow the exhaust gas flow, while bigger droplets interpenetrates the gas flow and hit the opposite wall. The simulation model delivers a critical diameter, which represents the biggest possible droplet, which is deflected by the gas flow and will not hit the opposite wall.

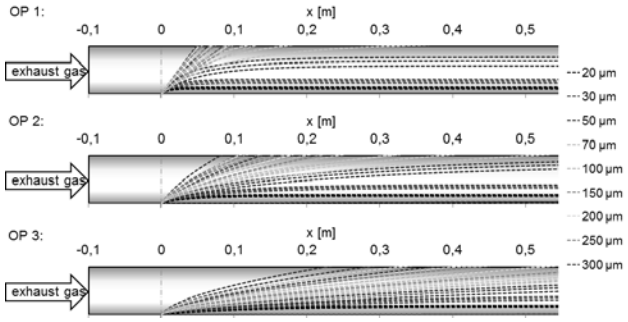

Fig. 8: Trajectories of droplets, off-centered coflow-injection, exit velocity 15 m/s, cone angle 16°, injection angle 45°

The comparison of the critical diameter with the droplet size distribution of the initial spray provides the precise percentage of free-moving droplets, without wall contact inside the mixing section, figure 9.

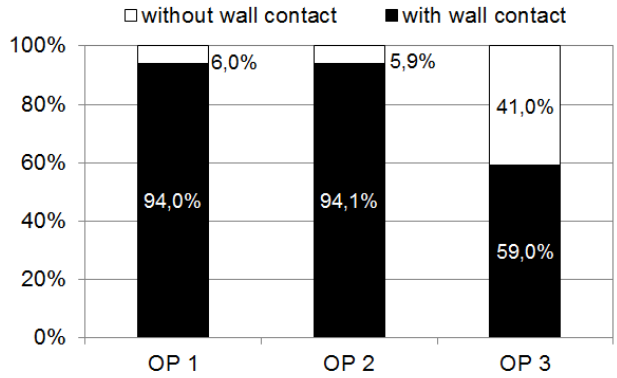

Fig. 9: Percentage of droplets with and without wall contact for an off-centered coflow injection

The geometry of this reference scenario results in predominant wall contact of the injected UWS with percentages between 59% and 94,1%.

4.4.2 Counter flow-injection, off-centered

In case of a counter flow injection, droplets will be injected against the gas flow and its motion get reversed by the acting gas force. The trajectories of the considered droplet sizes are depicted in figure 10.

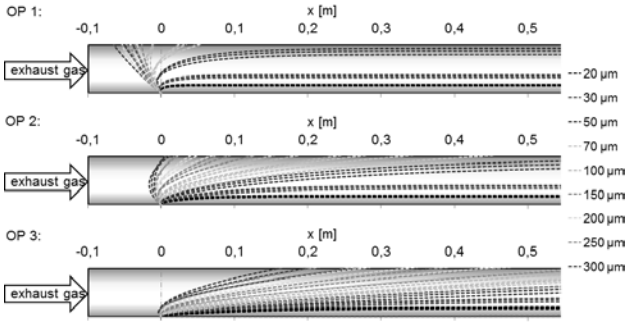

Fig. 10: Trajectories of droplets, off-centered counter flow-injection, exit velocity 15 m/s, cone angle 16°, injection angle 135°

The counter flow-injection from the pipe wall shows larger percentages of wall contact. This is due to the fact that the droplets get decelerated and accelerated in axial direction by the gas flow. This results in an increased residence time of the droplets in the mixing section which increases the penetration depth and hence the percentage of wall contact, figure 11.

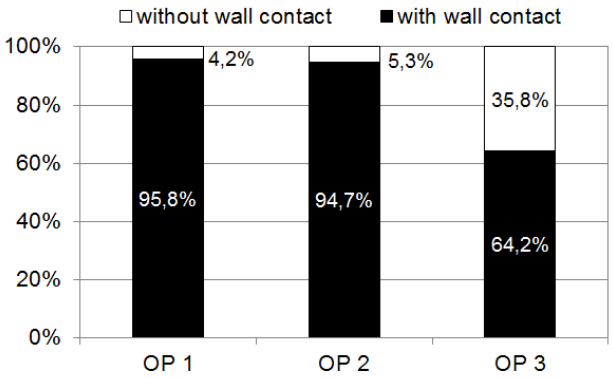

Fig. 11: Percentage of droplets with and without wall contact for an off-centered counter flow injection

The consequent comparison of the coflow and counterflow injection from the off-centered position allows the implication that the counter flow injection does not supply advantages in avoiding wall contact.

4.4.3 Coflow-injection, centered

The ensuing investigations show the theoretical potential of centered injections position for co- and counter flow injection. Figure 12 illustrates the trajectories of the droplets for the centered coflow injection and a simple visual comparison with the off-centered coflow-injection in figure 8 demonstrates the advantages of this injection position.

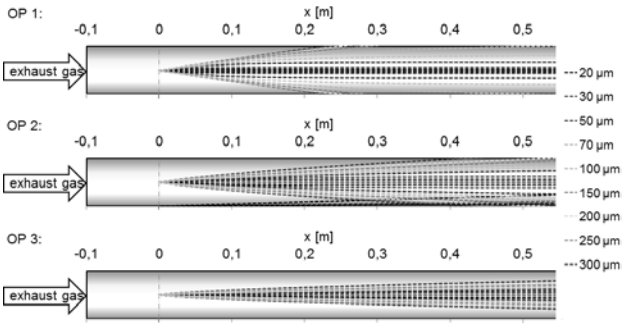

Fig. 12: Trajectories of droplets, centered coflow-injection, exit velocity 15 m/s, cone angle 16°, injection angle 0°

The percentage of droplets which suffer wall contact is reduced significantly, figure 13. Especially in operation point three, the droplets get deflected completely by the exhaust gas and prevent wall contact successfully.

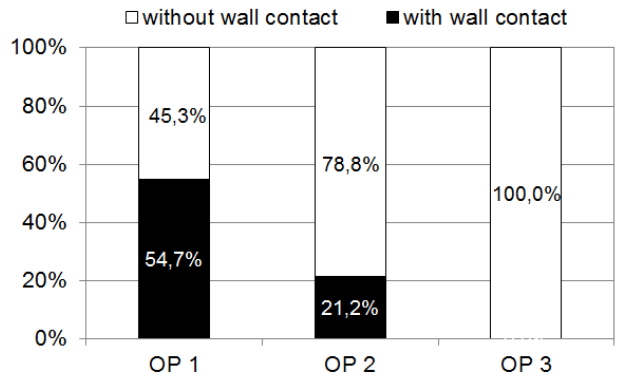

Fig. 13: Percentage of droplets with and without wall contact for a centered coflow injection

4.4.4 Counter flow-injection, centered

The last variant is represented by a centered counter flow-injection, figure 14. In case of low gas velocities, e.g. OP 1 the droplets are able to penetrate the exhaust gas in axial direction considerably, before the deflection by the gas flow occurs. This fact increases the residence time of the droplets in the mixing section, but results in higher percentage of wall contact compared to the centered coflow-injection.

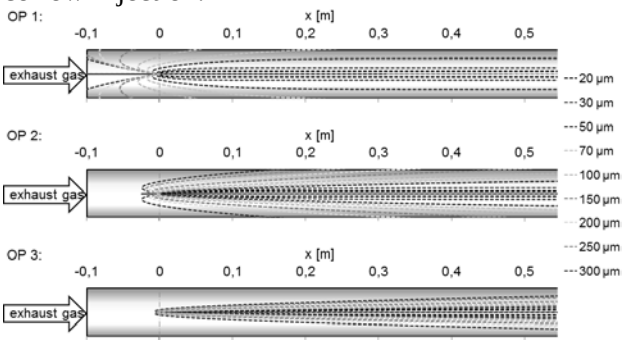

Fig. 14: Trajectories of droplets, centered counter flow-injection, exit velocity 15 m/s, cone angle 16°, injection angle 180°

Figure 15 pictures the percentages of the droplets with and without wall contact for the centered counter flow-injection.

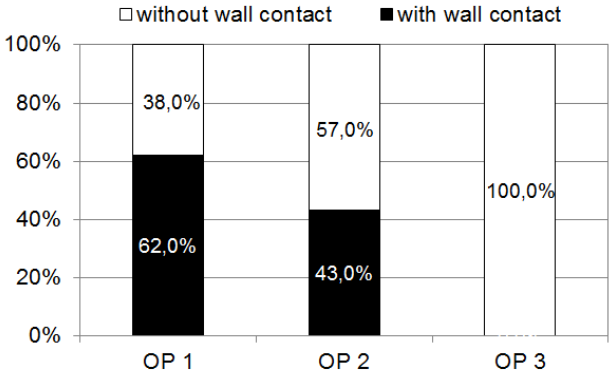

Fig. 15: Percentage of droplets with and without wall contact for a centered counter flow injection

4.5 Comparison and discussion of variants

In the sequence of the potential analysis to reduce wall contact, the observed variants can be re-ordered like stated below:

1. Centered coflow-injection
2. Centered counter flow-injection
3. Off-centered coflow-injection
4. Off-centered counter flow-injection

Another aspect which must be taken into account is the evaporation rate. The ideal case would be a complete evaporation of water out of the UWS-droplet and an entire thermolysis in this order. Figure 16 shows comparatively the weight losses of droplets with an initial diameter of 50 µm for the four geometries in relation to the residence time inside the mixing section.

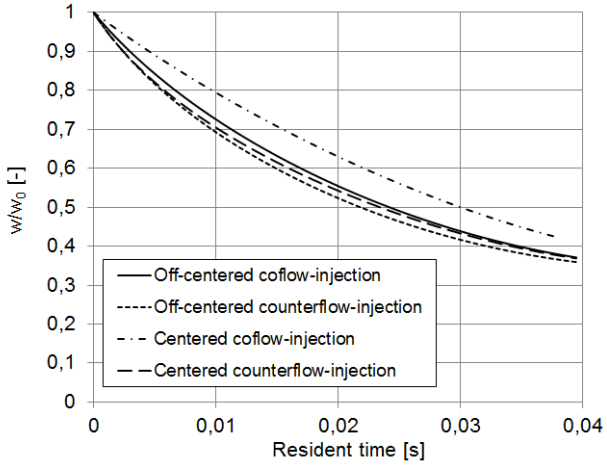

Fig. 16: Loss of droplet`s weight for the investigated injection geometries during the flight phase in the mixing section

The resulting residence times of the droplets before entering the catalytic converter differs due to the injection variants and the differences in the travelled path lengths of the droplets.

Another factor for differences in the weight loss is that the relative velocity between the droplet and the surrounding exhaust gas depends on the injection geometry. The highest relative velocities and further the highest weight losses can be expected for counter flow-injections. This is reasoned by higher Reynolds numbers, according to Eq. (14) and Eq. (15).

$$\vec{u}_{rel} = \vec{u}_{gas} - \vec{u}_{dr} \tag{14}$$

$$Re_{dr} = \frac{\rho_{gas} * |\vec{u}_{rel}| * D_{dr}}{\mu_{gas}} \tag{15}$$

High Reynold numbers are responsible for increasing heat transition and mass transfer coefficients k_w and k_m, and is a key factor for high heat transitions and mass transfers, compare to Eq. (9) and Eq. (13).

For none of the investigated geometries could be confirmed that evaporation and thermolysis are completed inside the mixing section. The demixing of UWS and the evaporation of water was completed by achieving a mass fraction of 0,325 that is equal to the initial mass fraction of urea in the UWS. This implicates that liquid droplets enter the catalytic converter and reduce the entire efficiency of the SCR process chain.

4 Conclusion

For the description of the droplets' trajectories in mixing sections of SCR-systems an empirically validated numeric model was developed, which takes in contrary to previous surveys, the loss of the droplets` weight due to evaporation of water and thermal decomposition of urea into account. The model for the droplets` motion was extended by an evaporation model for binary fluids and by a kinetic approach to describe furthermore the thermolysis of urea. This model is able to determine the exact position of the free-flying droplet, the droplets` velocity, the composition and its current temperature.

For a droplet which moves freely in a hot gas stream could be proved that weight losses due to evaporation or thermal decomposition are responsible for a significant change of the trajectories compared to droplets with constant mass or pure water droplets. Numerical models which use the characteristic data of water to approach the behavior of UWS result also in distinct inaccuracies.

The simulation can predict the percentage of droplets which suffer wall contact for various operation points and geometries. A potential analysis of coflow or counter flow-injections, of centered or off-centered-injections show significant advantages of coflow- and centered injections.

Due to challenges in the technical implementation of centered injection positions the coflow injection from the pipe wall seems to be the most applicable variant for realizing the considered SCR-mixing section.

References:

[1] M. Weißbäck, „Erfüllung zukünftiger Emissionsanforderungen für Diesel SUV`s," Forschungsgesellschaft Kraftfahrwesen mbH Aachen, 15. Aachener Kolloquium Fahrzeug- und Motorentechnik, Tagungsband Nr. 1506, 2006.

[2] G. Merker, Verbrennungsmotoren, Wiesbaden: B. G. Teubner, ISBN-10 3-8351-0080-7, 2006.

[3] F. Birkhold, „Selektive katalytische Reduktion von Stickoxiden in Kraftfahrzeugen: Untersuchung der Einspritzung von Harnstoff-Wasserlösung," Dissertation an der Universität Stuttgart, 2007.

[4] S. Fischer, AdBlue-Aufbereitung vor dem SCR-Katalysator, Entwicklung und Validierung eines 3D-Simulationsmodells, Vortrag zum Forschungsprojekt am Institut für Fahrzeugantriebe und Automobiltechnik der TU Wien, 30.6.2009, 2009.

[5] W. Ranz und W. Marshall, Evaporation from drops, Chem. Eng. Prog., Vol. 48, 1952.

[6] S. Yim, Decomposition of Urea into NH3 for the SCR-Process, Industrial & Engineering Chemistry Research: American Chemical Society, Volume 43, Page 4856-4863, 2004.

[7] G. Wozniak, Zerstäubungstechnik, ISBN 3-540-41170-4: Springer, 2003.

[8] L. Möltner, Tropfen/Abgas- und Tropfen/Wandinteraktionen von AdBlue bei der selektiven katalytischen Reduktion von Stickoxiden, Fortschritt-Berichte VDI Reihe 12 Verkehrstechnik/Fahrzeugtechnik Nr. 785, VDI Verlag Düsseldorf, ISBN 978-3-18-378512-4, 2014